Inorganic Chemistry

pubs.acs.org/IC

Article

Methyl Effects on the Stereochemistry and Reactivity of PPP-Ligated Iron Hydride Complexes

Bedraj Pandey, Jeanette A. Krause, and Hairong Guan*

Cite This: *Inorg. Chem.* 2023, 62, 967−978

Read Online

ACCESS | Metrics & More | Article Recommendations | Supporting Information

ABSTRACT: Iron dihydride complexes are key intermediates in many iron-catalyzed reactions. Previous efforts to study molecules of this type have led to the discovery of a remarkably stable *cis*-FeH_2 complex, which is supported by bis[2-(diisopropylphosphino)phenyl]phosphine ($^{iPr}PP^HP$) along with CO. In this work, the hydrogen on the central phosphorus has been replaced with a methyl group, and the corresponding iron carbonyl dichloride, hydrido chloride, and dihydride complexes have been synthesized. The addition of the methyl group favors the *anti* configuration for the Me−P−Fe−H moiety and the *trans* geometry for the H−Fe−CO motif, which is distinctively different from the $^{iPr}PP^HP$ system. Furthermore, it increases the thermal stability of the dihydride complex, *cis*-($^{iPr}PP^{Me}P$)Fe(CO)H_2 ($^{iPr}PP^{Me}P$ = bis[2-(diisopropylphosphino)phenyl]methylphosphine). The variations in stereochemistry and compound stability contribute greatly to the differences between the two PPP systems in reactions with PhCHO, CS_2, and HCO_2H.

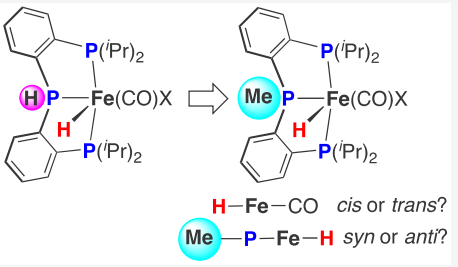

INTRODUCTION

Adding a methyl group to an existing molecule, which may be perceived as a trivial structural modification, can have a profound impact on the reactivity. Methylating a small-molecule drug in particular can result in as much as a 100-fold increase in efficacy through the alteration of protein−ligand binding.[1] In the field of transition-metal catalysis, replacing a metal-bound NH group with an NMe group has been frequently used to probe the roles that the protic hydrogen may or may not play (e.g., transfers H^+, stabilizes the transition states).[2] The methylated catalysts sometimes outperform the nonmethylated ones, an outcome that has been attributed to improved catalyst stability.[3] In our view, the methyl effects are likely more nuanced and complex than previously thought. To fully understand how the added methyl group can enhance or diminish the catalytic activity, detailed studies of the individual steps are needed.

We have recently reported a *cis*-FeH_2 complex as well as its monohydride derivatives supported by (o-^{i}Pr$_2$PC_6H_4)$_2$PH (abbreviated here as $^{iPr}PP^HP$) along with CO.[4] This specific dihydride complex is remarkably stable against H_2 elimination but capable of catalyzing reactions such as the Tishchenko reaction, the hydrogenation of PhCHO, the dehydrogenation of $PhCH_2OH$, and the additive-free dehydrogenation of formic acid. The spatial arrangement of the hydride(s) in relation to CO and $^{iPr}PP^HP$, particularly with respect to the orientation of the PH hydrogen, is not always fixed. For example, the freshly isolated ($^{iPr}PP^HP$)FeH(CO)Cl exists as a 82:18 mixture of *anti* and *syn* isomers (defined based on the H−P−Fe−H configuration), both with a *cis* relationship between the hydride and CO (Scheme 1). However, the composition changes over time, producing a second *syn* isomer that features a *trans* H−Fe−CO motif. The protonation of *cis*-($^{iPr}PP^HP$)-Fe(CO)H_2 with HCO_2H, on the other hand, results in a complete shift of the coordination site for CO.

Scheme 1. Configurational Lability of H−Fe−CO in $^{iPr}PP^HP$-Ligated Complexes

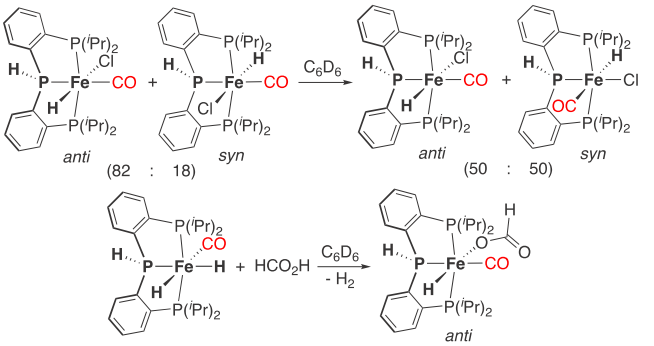

We surmised that introducing a methyl group to the central phosphorus donor could modify the steric environment around iron and the net charge on the phosphorus substituent,[5] which in turn could influence how the remaining ligands (CO, H, and another X-type ligand) are arranged in the coordination sphere. The variation of stereochemistry, coupled with the

Received: October 28, 2022
Published: January 5, 2023

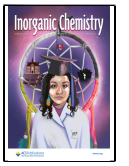

https://doi.org/10.1021/acs.inorgchem.2c03803
Inorg. Chem. 2023, 62, 967−978

change in electron density at the iron center,[6] could make the iron hydride complexes react differently. The objective of this work is thus to examine these methyl effects in both stoichiometric and catalytic reactions. Considering that iron dihydride species[7] are key intermediates in many catalytic processes but, due to their low stability, often difficult to study, we focused this work specifically on comparing the reactivity of *cis*-(^{iPr}PP^{H}P)Fe(CO)H_2 with its *P*-methylated analog, *cis*-(^{iPr}PP^{Me}P)Fe(CO)H_2 (^{iPr}PP^{Me}P = (*o*-^{i}Pr$_2$PC$_6$H$_4$)$_2$PMe).

RESULTS AND DISCUSSION

Synthesis and Isomerization of Iron Monohydride Complexes. The first step in our synthesis involved the mixing of ^{iPr}PP^{Me}P (a ligand developed by Lee and coworkers[8]) with $FeCl_2$ followed by exposure to CO, which produced *trans*-(^{iPr}PP^{Me}P)Fe(CO)Cl_2 (**1**) in high yield (Scheme 2). The ligation of ^{iPr}PP^{Me}P and CO was evident

Scheme 2. Synthesis of the Iron Carbonyl Dichloride Complex

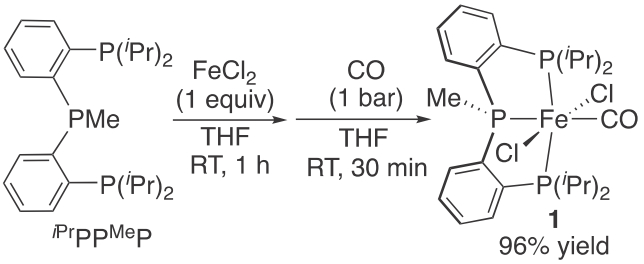

from the NMR and IR spectra of the isolated product. The most unusual spectroscopic property is that, upon binding to iron, the central phosphorus responds with a coordination chemical shift significantly larger than that observed for the periphery phosphorus (134.7 ppm for $\Delta\delta_{PMe}$ vs 72.6 ppm for $\Delta\delta_{P(iPr)2}$; see Table 1), resulting in a switch of their relative

Table 1. Comparison of the ^{31}P NMR Coordination Chemical Shifts ($\Delta\delta = \delta_{complex} - \delta_{ligand}$)

	central phosphorus (PH/PMe)			periphery phosphorus (P^iPr_2)		
	$\delta_{complex}$	δ_{ligand}	$\Delta\delta$	$\delta_{complex}$	δ_{ligand}	$\Delta\delta$
^{iPr}PP^{Me}P (in CD_2Cl_2)	98.1	−36.6	134.7	70.2	−2.4	72.6
^{iPr}PP^{H}P(in $CDCl_3$)	72.9	−49.5	122.4	74.8	0.0	74.8

positions in the ^{31}P NMR spectra. Going from ^{iPr}PP^{H}P to *trans*-(^{iPr}PP^{H}P)Fe(CO)Cl_2, the *P*H resonance is also shifted more than the *P*(^{i}Pr)$_2$ resonance but not enough to overtake the latter (i.e., the *P*H resonance is always more upfield). Within the same class of metal-phosphine complexes, coordination chemical shifts can correlate linearly with the M−P bond enthalpies and distances.[9] The results here suggest that the PME group of ^{iPr}PP^{Me}P binds to iron more strongly than the PH group of ^{iPr}PP^{H}P. The overall electronic properties of the two PPP-type ligands may be gauged from the ν_{CO} values for the corresponding Fe(CO)Cl_2 complexes. Compound **1** dissolved in CH_2Cl_2 shows a CO stretching band (1946 cm^{-1}) at a lower frequency than *trans*-(^{iPr}PP^{H}P)Fe(CO)Cl_2 (1974 cm^{-1}), indicating that the extent of π backdonation to CO is greater with the ^{iPr}PP^{Me}P system. In other words, the methylated ligand is in fact more electron-rich than ^{iPr}PP^{H}P.

The bond metrics of **1** revealed by X-ray crystallography (Figure 1) are consistent with the ^{31}P NMR trend. Compared

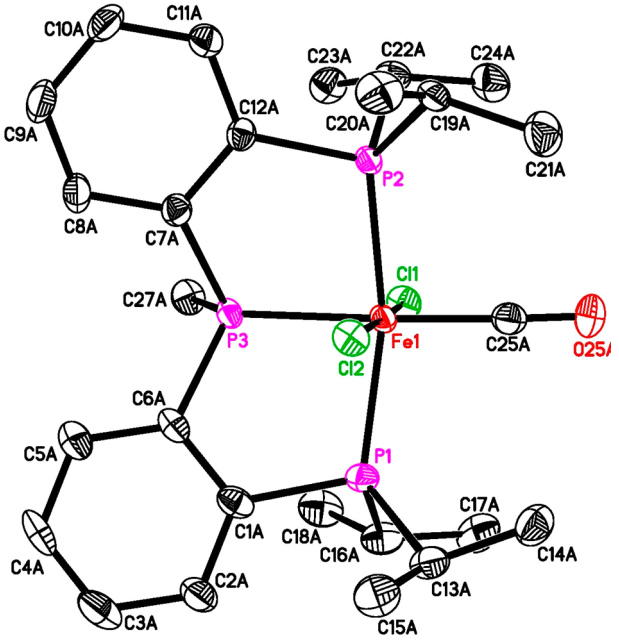

Figure 1. ORTEP of **1** at the 50% probability level (there are two independent molecules in the lattice and only molecule A is shown here; all hydrogen atoms are omitted for clarity). Selected bond lengths (Å) and angles (deg): Fe1−Cl1 2.3210(10), Fe1−Cl2 2.3218(10), Fe1−C25A 1.789(4), Fe1−P1 2.2878(10), Fe1−P2 2.2777(10), Fe1−P3 2.2238(11), C25A−O25A 1.153(5); Cl1−Fe1−Cl2 177.54(5), P1−Fe1−P2 163.36(4), P1−Fe1−P3 84.56(4), P2−Fe1−P3 84.38(4), P3−Fe1−Cl1 91.19(4), P3−Fe1−Cl2 86.37(4), P3−Fe1−C25A 175.12(13), and Fe1−C25A−O25A 173.2(4).

to the ^{iPr}PP^{H}P system,[4] the methylated ligand forms a shorter Fe−P bond with the central phosphorus (~0.015 Å) and longer Fe−P bonds with the periphery phosphorus (~0.02 Å). Interestingly, the Fe−Cl and Fe−CO bond distances are virtually unaffected by the methylation. The isopropyl groups seem to exert the most steric pressure on the chloride ligands, especially for the one that resides *anti* to PMe/PH.[10] Despite having a shorter Fe−$P_{central}$ bond and an additional methyl group in the vicinity of iron, the elongation of the Fe−$P_{periphery}$ bonds renders the two P3−Fe−Cl angles more equal (86.37(4) and 91.19(4)° for the molecule shown in Figure 1, 87.63(4) and 90.13(4)° for the independent molecule not shown). The steric clash between the isopropyl groups and chloride ligands is exacerbated in *trans*-(^{iPr}PP^{H}P)Fe(CO)Cl_2, forcing the Cl−Fe−Cl axis to slant with two drastically different $P_{central}$−Fe−Cl angles (81.20(2) and 102.71(2)°).[4] Another noticeable structural change is the $P_{central}$−Fe−CO angle, which is more linear in **1** (175.12(13) or 175.54(16) vs 169.59(7)° in *trans*-(^{iPr}PP^{H}P)Fe(CO)Cl_2). The CO ligand in the methylated complex is, however, bent toward the *syn* chloride (i.e., Cl1 in Figure 1) with an Fe−C−O angle of 173.2(4) or 173.9(4)°, in contrast to the nearly linear Fe−C−O angle observed with *trans*-(^{iPr}PP^{H}P)Fe(CO)Cl_2 (178.1(2)°, slightly bent toward the *anti* chloride). The deviation of Fe−C−O from linearity has been previously reported for five-

https://doi.org/10.1021/acs.inorgchem.2c03803
Inorg. Chem. 2023, 62, 967−978

coordinate iron complexes, and the origin could be electronic.[11] The C−O bond distance determined for **1** (1.153(5) or 1.146(6) Å) is indeed longer than that measured for *trans*-(^{iPr}PP^{H}P)Fe(CO)Cl$_2$ (1.116(3) Å), consistent with more π back-donation to CO for the methylated complex. However, a close inspection of the space-filling model of **1** and *trans*-(^{iPr}PP^{H}P)Fe(CO)Cl$_2$ suggests that the degree/direction of CO bending could simply be a result of avoiding the steric repulsion from the isopropyl groups. It is worth mentioning that environmental effects on CO bending are well documented for the myoglobin or hemoglobin CO adduct.[12]

Substituting hydride for one chloride ligand would yield a monohydride complex with the formula (^{iPr}PP^{Me}P)FeH(CO)Cl (**2**). In principle, **2** has six geometric isomers that differ by the spatial arrangement of H/CO/Cl and the orientation of the PMe methyl group (Chart 1). The chemical shift value for

Chart 1. Geometric Isomers of (^{iPr}PP^{Me}P)FeH(CO)Cl

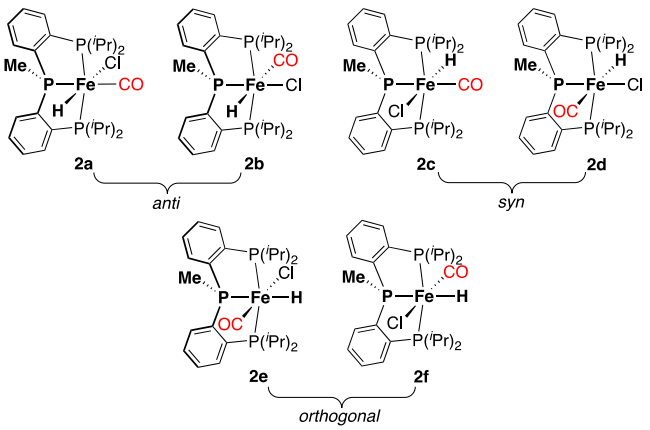

the hydride can be used to discern what type of ligand occupies its *trans* site,[13] while nuclear Overhauser effect spectroscopy (NOESY) experiments can be carried out to distinguish the *syn* isomers from the *anti* and *orthogonal* isomers. The ^{31}P NMR resonance for the central phosphorus can also provide spectroscopic information about its opposing ligand.

The ligand substitution reaction was accomplished by treating **1** with 1 equiv of NaBH$_4$ in ethanol, which yielded an isomeric mixture of **2**. Pure **2a** was isolated following recrystallization from toluene−pentane. In CD_2Cl_2, **2a** displays a hydride resonance at δ −26.69 (a triplet of doublets), consistent with an iron hydride *trans* to a chloride ligand.[4,13g−i] The lack of NOE correlation between the P*Me* and Fe*H* resonances rules out the possibility of having a *syn* isomer like **2c**. The *trans* H−Fe−Cl motif and the *anti* Me−P−Fe−H configuration were more firmly established by X-ray crystallography (Figure 2). Compared to the structure of **1**, the Fe−P bonds in **2a** are shortened substantially (by ∼0.04 Å for the Fe−P$_{central}$ bond and ∼0.08 Å for the Fe−P$_{periphery}$ bonds), presumably due to the removal of a bulky chloride ligand. The larger extent of bond contraction with the periphery phosphorus is also reflected by the ^{31}P NMR data (in CD_2Cl_2), now showing an AB$_2$ spin pattern with the P(^{i}Pr)$_2$ resonance (δ 104.1) found in the more downfield region than the P*Me* resonance (δ 100.2). (For a more detailed analysis of the coordination chemical shifts, see Figure S41.) Additional structural adjustments include a more folded PPP ligand framework (P$_{periphery}$−Fe−P$_{periphery}$ angle: 152.07(4)° in **2a** vs 163.36(4) or 163.79(4)° in **1**) and a longer Fe−Cl bond

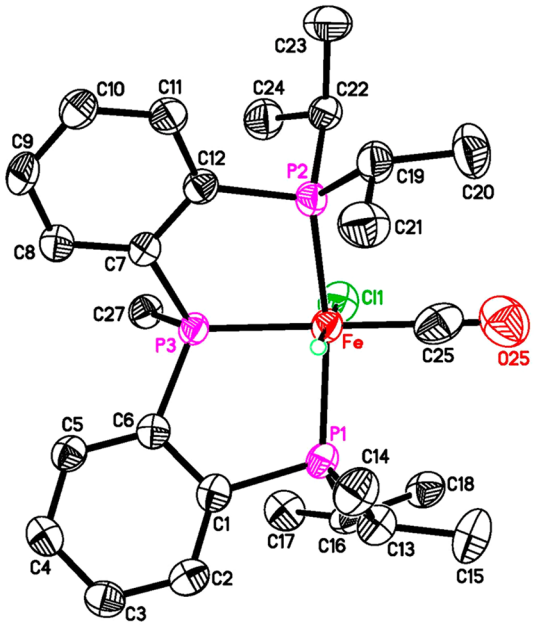

Figure 2. ORTEP of **2a** at the 50% probability level (all hydrogen atoms except the one bound to iron are omitted for clarity). Selected bond lengths (Å) and angles (deg): Fe−Cl1 2.3829(14), Fe−H 1.506(43), Fe−C25 1.817(6), Fe−P1 2.1956(11), Fe−P2 2.2024(10), Fe−P3 2.1875(10), C25−O25 1.071(6); P1−Fe−P2 152.07(4), P1−Fe−P3 86.83(4), P2−Fe−P3 85.69(4), P3−Fe−Cl1 92.66(4), P3−Fe−C25 179.64(14), and Fe−C25−O25 175.0(5).

(2.3829(14) Å in **2a** vs 2.3210(10) Å or 2.3227(11) Å in **1**), which can be explained by the small size and strong *trans* influence of the hydride, respectively. Unlike the iron carbonyl dichloride complexes discussed earlier, **2a** and its non-methylated analog, *anti*-(^{iPr}PP^{H}P)FeH(CO)Cl (the isomer with the same ligand arrangement as **2a**), show very little structural variation in the Fe−P bond distances and the bond angles about iron. However, the Fe−Cl and Fe−CO bonds are noticeably longer in **2a**, by 0.02 and 0.05 Å, respectively. The additional methyl group evidently steers the isopropyl groups to adopt conformations that more sterically hinder the chloride and CO.

While the structural differences between **2a** and *anti*-(^{iPr}PP^{H}P)FeH(CO)Cl are small,[14] their reactivity differs greatly. When a solution of **2a** in CD_2Cl_2 was heated to 50 °C, **2a** gradually isomerized to **2b** and reached equilibrium in 48 h (Scheme 3). The hydride resonance for the new isomer was located at δ −7.32 (a doublet of triplets), indicating that CO had already shifted to its *trans* site.[13a−c,g] As expected for an *anti* isomer, **2b** showed no NOE correlation between the P*Me* and Fe*H* resonances. Fortunately, **2b** crystallized selectively from a C_6D_6 solution of **2a**/**2b**, providing the opportunity to further confirm the proposed structure (Figure 3). During the isomerization of **2a** to **2b**, another isomer was also detected by NMR, although its quantity was too low (<2%) to allow further structural interrogation by NOESY. Given the chemical shift value for the hydride (δ −25.61, a doublet of triplets), we tentatively propose that the third isomer is **2c**. ^{31}P NMR chemical shifts are usually sensitive to the bond angles about the phosphorus center. The differences in bond angles among the geometric isomers are small enough to allow us to judge what ligand is *trans* to each phosphorus simply based on the ^{31}P NMR chemical shift value. (See Figure

https://doi.org/10.1021/acs.inorgchem.2c03803
Inorg. Chem. 2023, 62, 967−978

Scheme 3. Isomerization of the PPP-Ligated Iron Monohydride Complexes

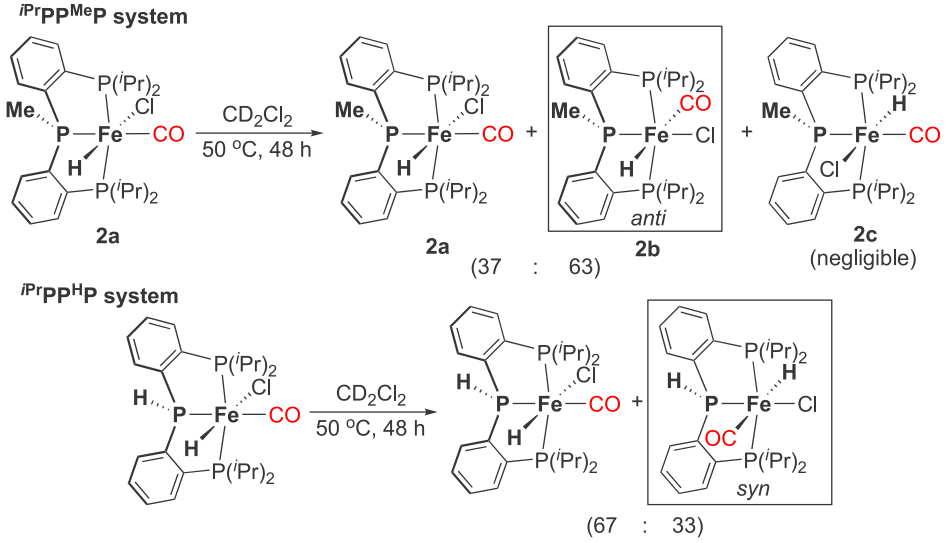

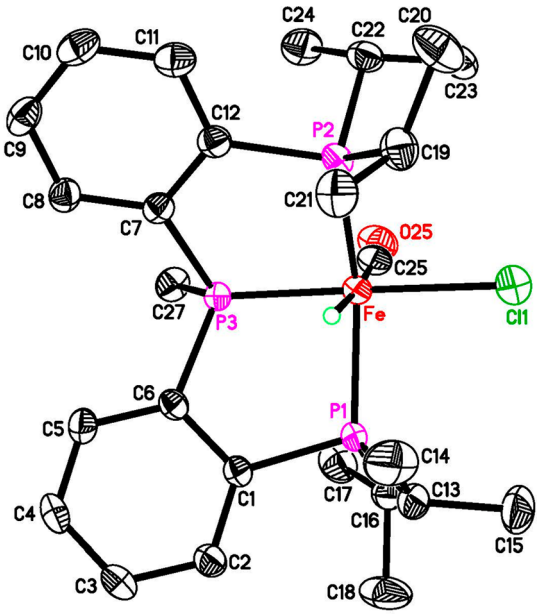

Figure 3. ORTEP of **2b** at the 50% probability level. (All hydrogen atoms except the one bound to iron are omitted for clarity.) Selected bond lengths (Å) and angles (deg): Fe−Cl1 2.3689(8), Fe−H 1.564(30), Fe−C25 1.841(5), Fe−P1 2.2255(7), Fe−P2 2.2052(8), Fe−P3 2.1443(7), C25−O25 0.929(4); P1−Fe−P2 145.73(3), P1−Fe−P3 86.62(3), P2−Fe−P3 86.89(3), P3−Fe−Cl1 175.42(3), P3−Fe−C25 95.22(10), and Fe−C25−O25 173.8(4).

S41 for details.) The observation that **2b** is thermodynamically more stable than **2a** is somewhat surprising. One may have anticipated that the two strongly *trans*-influencing ligands, namely, the hydride and CO, should avoid being *trans* to each other. It is possible that the isomerization reaction is driven by the relief of steric repulsion between the PMe methyl group and the chloride. For comparison purposes, the geometric isomerization of our previously reported *anti*-(^{iPr}PP^{H}P)FeH(CO)Cl[4] was re-examined under the same conditions presented here (in CD_2Cl_2 at 50 °C). The striking difference between the two ligand systems is the preferred Me/H−P−Fe−H configuration following the shift of CO to the hydride's *trans* site (see the boxed structures in Scheme 3). For the ^{iPr}PP^{H}P system, the preference for the *syn* configuration is likely due to a favorable electrostatic interaction between the protic PH hydrogen ($H^{\delta+}$) and the hydride ($H^{\delta-}$).[15] Such interaction is diminished or absent in the methylated system, and sterically, it is preferable to place CO in the coordination site adjacent to the PMe methyl group.

In studying the reaction of *trans*-(^{R}PN^{H}P)Fe(CO)Cl$_2$ (^{R}PN^{H}P = $(R_2PCH_2CH_2)_2NH$, R = ^{i}Pr or Cy) with $^{n}Bu_4NBH_4$, Hazari and Schneider proposed that the NH group could direct the delivery of H^- to the adjacent coordination site, giving *syn*-(^{R}PN^{H}P)FeH(CO)Cl as the kinetic product.[13g] Subsequent isomerization was shown to change the H−N−Fe−H configuration from *syn* to *anti*, although the *cis* geometry for H−Fe−CO was preserved. This study prompted us to monitor the progress of the monohydride formation in both PPP systems with the objective being to understand how **1** and *trans*-(^{iPr}PP^{H}P)Fe(CO)Cl$_2$ initially react with $NaBH_4$ (Scheme 4). To our surprise, the ^{iPr}PP^{Me}P system yielded **2b** as the kinetic product, which underwent isomerization slowly to afford a mixture of **2a** and **2b**. Because the substitution reaction was performed in ethanol-d_6, deuterium was incorporated into the hydride position, showing isotopically shifted ^{31}P NMR resonances split by the ^{2}H nucleus (i.e., featuring 1:1:1 triplets). In contrast, the kinetic product for the ^{iPr}PP^{H}P system was identified as *syn*-(^{iPr}PP^{H}P)FeH(CO)Cl, in which CO remained *trans* to the central phosphorus. This hydride species then started to isomerize to its *anti* isomer and a second *syn* isomer bearing a *trans* H−Fe−CO motif. In this case, deuterium was incorporated not only into the hydride position but also into the PH position. The difference in kinetic products suggests that the two PPP systems follow distinctively different mechanisms. The iron-bound PH group may have favorable electrostatic interactions with $NaBH_4$, which direct the delivery of H^- to iron in a similar fashion as proposed for the PNP system.[13g] The iron-bound PMe group lacks such ability due to increased electronegativity for the carbon and for the methyl group as a whole.[5] To explain the formation of **2b** as a kinetic product, we hypothesize that, for the ^{iPr}PP^{Me}P system, the first step of the reaction involves solvolysis[16] of the sterically more accessible Fe−Cl bond, which is mainly dictated by how the the PPP ligand framework folds (Scheme 5). The resulting

https://doi.org/10.1021/acs.inorgchem.2c03803
Inorg. Chem. 2023, 62, 967−978

Scheme 4. Reactions of the Iron Carbonyl Dichloride Complexes with $NaBH_4$

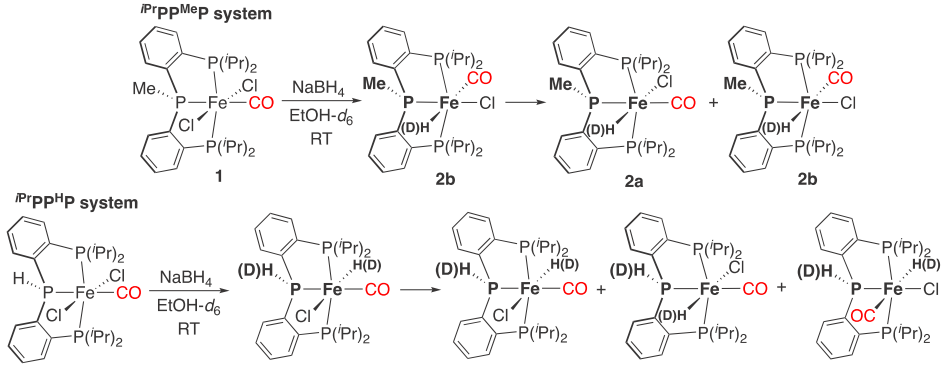

Scheme 5. Plausible Mechanism Explaining the Formation of 2b as a Kinetic Product

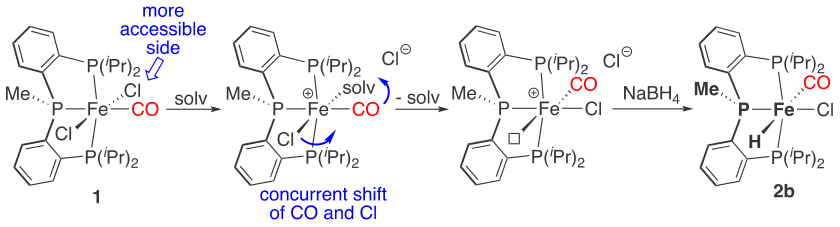

intermediate provides the configurational lability that allows the strongly *trans*-influencing CO to be *trans* to a vacant coordination site. Subsequent H^- transfer from $NaBH_4$ would yield **2b** exclusively.

Synthesis of the Iron Dihydride Complex. When $NaBH_4$ was added in large excess to a solution of **1** in ethanol, both chloride ligands were replaced with a hydride, leading to the isolation of *cis*-(^{iPr}PP^{Me}P)Fe(CO)H_2 (**3**) (Scheme 6).

Scheme 6. Synthesis of the Iron Carbonyl Dihydride Complex

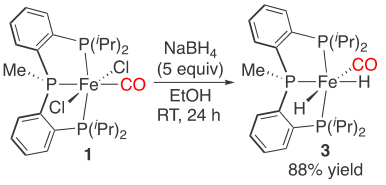

Similar to our previously reported ^{iPr}PP^{H}P system,[4] the two hydride ligands prefer to be *cis* to each other, enabled by a shift of the coordination site for CO. At room temperature, **3** (in toluene-d_8) features two broad, rapidly exchanging hydride resonances at δ −9.97 and δ −14.09. The chemical shift values are consistent with hydrides *trans* to CO and a phosphorus donor, respectively. The exchange slows down significantly at −30 °C, at which point the broad resonances become two well-resolved triplets of doublets of doublets (Figure S16). These resonances coalesce at 45 °C ($\Delta G^{\ddagger}$ = 13.5 kcal/mol), comparable to the coalescence temperature determined for the hydride signals of *cis*-(^{iPr}PP^{H}P)Fe(CO)H_2 (50 °C, $\Delta G^{\ddagger}$ = 13.7 kcal/mol). This type of exchange process is well known for metal polyhydrides, likely involving an out-of-plane twist of the two hydrides via a dihydrogen complex-like transition state.[17] However, the dissociation of H_2 from **3** and *cis*-(^{iPr}PP^{H}P)Fe(CO)H_2 does not occur even at 80 °C, as evidenced by the lack of H/D exchange between the dihydride complexes and D_2 (1 bar). To further study the thermal stability, a solution of **3** in toluene-d_8 was held at 120 °C for 24 h and did not show signs of decomposition. Under the same conditions, a small but noticeable fraction of *cis*-(^{iPr}PP^{H}P)Fe(CO)H_2 decomposed to H_2 and a red precipitate. These results confirm that the methylated complex is thermally more stable, which can be rationalized based on the electronic effect (i.e., Fe(II) is better stabilized by the more electron-rich ligand, ^{iPr}PP^{Me}P).

Substituting hydride for the second chloride creates a less crowded environment around iron, resulting in further contraction of the Fe−$P_{periphery}$ bonds (by 0.04−0.07 Å when compared with **2b**). The key bond distances and angles, as summarized in Figure 4 and Table S12, are remarkably similar to those determined for *cis*-(^{iPr}PP^{H}P)Fe(CO)H_2. Minor variations may arise from the different conformations adopted by the isopropyl groups. Overall, the crystallographic data show that the structural differences between the two PPP systems diminish in the order of Fe(CO)Cl_2 > FeH(CO)Cl > Fe(CO)H_2 complexes.

Reactivity Differences between the Two PPP Systems. On steric grounds alone, we initially anticipated similar hydride reactivity for **3** and *cis*-(^{iPr}PP^{H}P)Fe(CO)H_2 because the two dihydride complexes have very similar structural parameters. In addition, the hydride ligands are *anti* or *orthogonal* to the methyl group or hydrogen on the central phosphorus or at sites that should not experience steric pressure directly from the PMe/PH functionality. The electronic argument would lead to the prediction that **3**, which bears a more electron-rich PPP ligand, should be more reactive than *cis*-(^{iPr}PP^{H}P)Fe(CO)H_2 because of the increased hydricity.

Insertion Reactions. Our previous study of the ^{iPr}PP^{H}P system demonstrated that, at 80 °C, *cis*-(^{iPr}PP^{H}P)Fe(CO)H_2 consumed PhCHO fully in 18 h to yield $PhCO_2CH_2Ph$ along with the regenerated dihydride complex.[4] Counterintuitively, the reaction of PhCHO with **3** under the same conditions was very sluggish, forming a trace amount of $PhCH_2OH$. It should be noted that free ligand was detected in the reaction of *cis*-(^{iPr}PP^{H}P)Fe(CO)H_2, implying that the conversion of PhCHO

https://doi.org/10.1021/acs.inorgchem.2c03803
Inorg. Chem. 2023, 62, 967−978

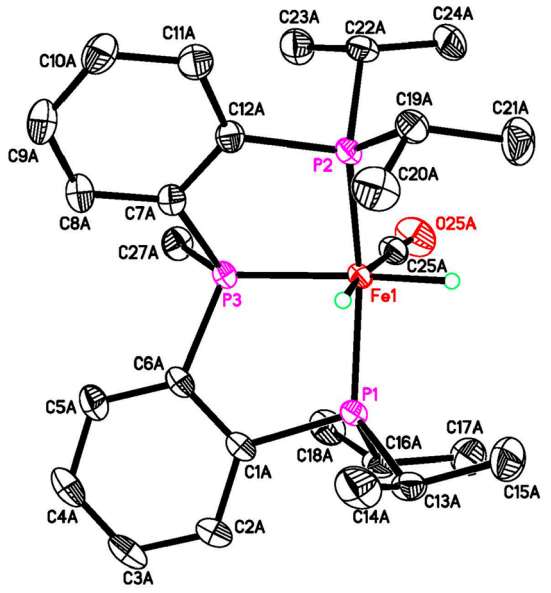

Figure 4. ORTEP of **3** at the 50% probability level (there are two independent molecules in the lattice and only molecule A is shown here; all hydrogen atoms except those bound to iron are omitted for clarity). Selected bond lengths (Å) and angles (deg): Fe1−H (*trans* to P3) 1.474(14), Fe1−H (*trans* to C25A) 1.480(14), Fe1−C25A 1.7485(13), Fe1−P1 2.1564(3), Fe1−P2 2.1619(3), Fe1−P3 2.1392(3), C25A−O25A 1.1601(16); P1−Fe1−P2 151.157(14), P1−Fe1−P3 87.945(13), P2−Fe1−P3 87.400(13), P3−Fe1−C25A 103.64(4), and Fe1−C25A−O25A 177.99(12).

to $PhCO_2CH_2Ph$ could potentially be promoted by some iron species degraded from the dihydride complex.

As an alternative carbonyl substrate to probe the reactivity difference, CO_2 (1 bar) was used to react with **3** and *cis*-($^{iPr}PP^{H}P$)Fe(CO)H_2. At room temperature or 80 °C, neither dihydride complex displayed any reactivity. Our attention was then turned to CS_2, a molecule that has more reactive π-bonds.[18] The treatment of **3** in C_6D_6 with 2 equiv of CS_2 showed a slow insertion reaction with the hydride *trans* to the central phosphorus (Scheme 7). In the first 24 h, the insertion product ($^{iPr}PP^{Me}P$)FeH(CO)(SCHS) (**4b**) formed cleanly, although the conversion was merely 48%. Extending the reaction time improved the conversion but at the same time led to the appearance of isomer **4a**, in which the coordination

Scheme 7. CS_2 Insertion with 3 and the Subsequent Isomerization Reaction

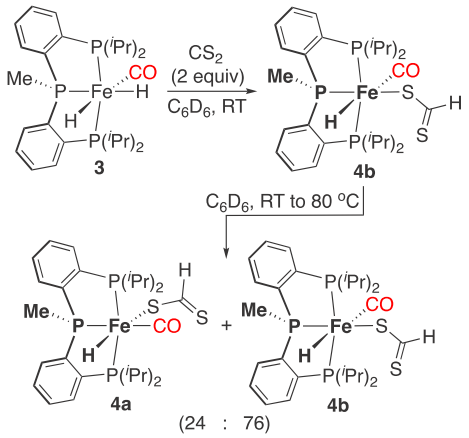

sites for the dithioformate and CO had been interchanged. The insertion process was accelerated at 80 °C and complete in 18 h, producing a 24:76 mixture of **4a** and **4b**. The remaining hydride for both isomers resisted further CS_2 insertion.

Recrystallization of the product mixture in toluene−THF at −30 °C afforded pure **4b**. The *trans*-H−Fe−CO motif was corroborated by a hydride resonance observed at δ −9.17 (a quartet, in C_6D_6), and the *anti*-Me−P−Fe−H configuration was established by NOESY (Figure S25). These structural features were further supported by X-ray crystallography (Figure 5). Considering that **4b** forms kinetically from the

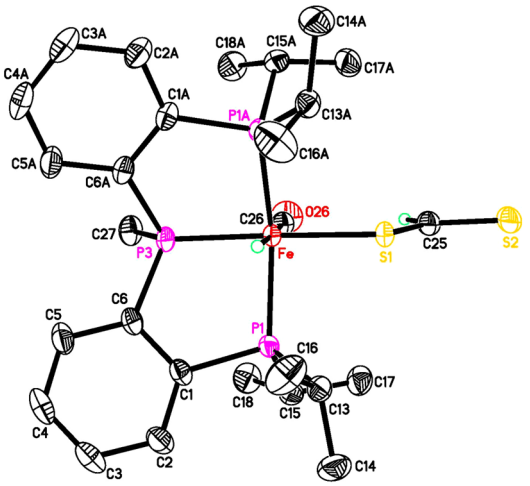

Figure 5. ORTEP of **4b** at the 50% probability level. (The cocrystallized toluene molecule and all hydrogen atoms except the one bound to iron and the one in dithioformate are omitted for clarity.) Selected bond lengths (Å) and angles (deg): Fe−H 1.479(21), Fe−C26 1.7657(18), Fe−P1 2.2189(3), Fe−P1A 2.2190(3), Fe−P3 2.1499(5), Fe−S1 2.2928(4), C26−O26 1.154(2), S1−C25 1.681(2), S2−C25 1.6545(19); P1−Fe−P1A 152.700(19), P1−Fe−P3 86.759(10), P1A−Fe−P3 86.757(10), P3−Fe−C26 94.33(6), Fe−C26−O26 177.25(17), P3−Fe−S1 169.40(2), and S1−C25−S2 126.31(14).

reaction of **3** with CS_2, comparing the structural parameters of **3** and **4b** can provide a glimpse into the adjustment that the supporting ligands need to make during the insertion process. To accommodate the newly formed dithioformate ligand, the Fe−$P_{periphery}$ bonds are elongated by 0.06 Å and the $P_{central}$−Fe−CO angle is compressed by 9.3°. The impact on the Fe−$P_{central}$ bond is minimal; the *trans* influence (bond contraction induced by the replacement of H with SCHS) is likely offset by the steric effect (bond elongation indirectly induced by SCHS).

Consistent with the result obtained from the insertion study (Scheme 7), pure **4b** dissolved in C_6D_6 was also found to isomerize to **4a** at 80 °C, forming an equilibrium mixture (**4a**/**4b** = 25:75) in 24 h. On the basis of the chemical shift value for the hydride (δ −19.22, a triplet of doublets) and the NOESY data (Figure S30), we propose that **4a** has a *trans*-H−Fe−SCSH motif and an *anti*-Me−P−Fe−H configuration. Like the chloride ligand in **2**, the dithioformate ligand prefers to be away from the PMe functionality (i.e., **4b** is thermodynamically more stable than **4a**), even if it means that the hydride and CO are forced to be *trans* to each other. The sequence of CS_2 insertion-geometric isomerization, to some degree, resembles the chemistry of *cis*-Fe(dmpe)$_2$H$_2$ (dmpe =

https://doi.org/10.1021/acs.inorgchem.2c03803
Inorg. Chem. 2023, 62, 967−978

$Me_2PCH_2CH_2PMe_2$) reported by Field and co-workers.[18b] The diphosphine system generates *cis*-Fe(dmpe)$_2$H(SCHS) at low temperatures (−33 to −53 °C) which, upon warming, quickly isomerizes to *trans*-Fe(dmpe)$_2$H(SCHS) to avoid having *trans*-H−Fe−PMe_2R. Here the $^{iPr}PP^{Me}P$ ligand provides sufficient rigidity and steric constraints that *trans*-H−Fe−SCHS is no longer favorable.

In C_6D_6, *cis*-($^{iPr}PP^{H}P$)Fe(CO)H_2 was shown to react with CS_2 ~20% faster than **3**. The marginally higher reactivity observed for the $^{iPr}PP^{H}P$ system may reflect a slightly less crowded transition state. While more reactive, *cis*-($^{iPr}PP^{H}P$)-Fe(CO)H_2 is less selective for the insertion process. According to the ^{1}H NMR spectra, at least seven different hydride species are formed, featuring two quartets at δ −8.79 and δ −9.36, two triplets of doublets at δ −18.27 and δ −19.21, and three ill-resolved multiplets at δ −18.6, δ −19.1, and δ −21.2. At this stage, we are unable to unambiguously establish their structures. It is possible that the insertion product ($^{iPr}PP^{H}P$)-FeH(CO)(SCHS) has six different geometric isomers analogous to those depicted in Chart 1. Other possibilities are isomers of ($^{iPr}PP^{H}P$)FeH(κ^S,κ^S-SCHS); the extrusion of an ancillary ligand following CS_2 insertion has been reported with other iron hydride complexes.[18d]

Protonation with Formic Acid. Another type of reactivity typically observed for iron hydride complexes is protonation of the hydride ligand with acids. Our previous work on *cis*-($^{iPr}PP^{H}P$)Fe(CO)H_2 showed that the reaction with HCO_2H produced H_2 and ($^{iPr}PP^{H}P$)FeH(CO)(OCHO), in which the CO position was completely shifted (Scheme 1).[4] The protonation reaction is too fast to differentiate the rates for the two PPP systems; however, the difference in stereochemistry is apparent. Upon mixing **3** with HCO_2H (5.5 equiv) in C_6D_6, a 24:76 mixture of **5a** and **5b** was obtained (Scheme 8). Both isomers are hydrogen bonded to HCO_2H, as

Scheme 8. Protonation with HCO_2H and the Subsequent Decarboxylation Reaction

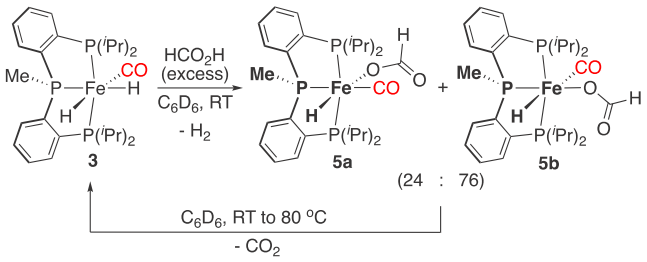

suggested by a continuous shift of the NMR signals (Fe*H*, OC*H*O, and phosphorus resonances) resulting from the dehydrogenation of HCO_2H to CO_2. When HCO_2H was near depletion, dihydride complex **3** began to emerge. At room temperature, the entire process required more than 2 days to reach completion, but at 80 °C, it needed only 30 min to fully convert HCO_2H and **5a**/**5b**. Of particular interest was that **5a** disappeared more rapidly than **5b**. It is unclear to us at the moment whether the decarboxylation of **5a** proceeds via *trans*-($^{iPr}PP^{Me}P$)Fe(CO)H_2 as a transient product or perhaps involves an initial isomerization of **5a** to **5b**. It should also be mentioned that, within 24 h of mixing (at room temperature), the free ligand $^{iPr}PP^{Me}P$ (~4%) was detected. Considering that **3** is thermally stable even at 120 °C, the decomposition likely originated from **5a**/**5b**.

The initial structural assignment of **5a**/**5b** was made on the basis of the NMR data. The major isomer **5b** displayed a hydride resonance in the region (δ −5.41 gradually shifted to δ −5.86, a doublet of triplets) consistent with the *trans* geometry for H−Fe−CO. The minor isomer **5a** showed a hydride resonance in the more upfield region (δ −28.24 gradually shifted to δ −27.85, a quartet), which resembles our previously characterized ($^{iPr}PP^{H}P$)FeH(CO)(OCHO)[4] as well as other *trans*-disposed hydrido formate complexes reported in the literature.[13h,19] Fractional crystallization of the initial protonation products at −30 °C (using toluene−THF as the solvent combination) produced single crystals of **5a**; despite repeated trials, the major isomer **5b** precipitated as an amorphous solid. Crystallographically characterized **5a** shows hydrogen-bonding interactions with two HCO_2H molecules (Figure 6). The

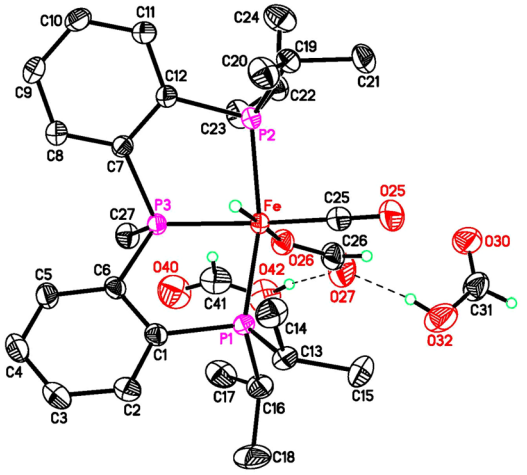

Figure 6. ORTEP of **5a**·2HCO_2H at the 50% probability level. (All hydrogen atoms except the one bound to iron and those in formate/formic acid are omitted for clarity.) Selected bond lengths (Å) and angles (deg): Fe−H 1.482(18), Fe−C25 1.7577(17), Fe−P1 2.2296(4), Fe−P2 2.2288(4), Fe−P3 2.2238(4), Fe−O26 2.0548(12), C25−O25 1.156(2), C26−O26 1.244(2), C26−O27 1.260(2); P1−Fe−P2 160.084(17), P1−Fe−P3 84.874(15), P2−Fe−P3 85.150(15), P3−Fe−C25 168.47(6), Fe−C25−O25 177.53(17), P3−Fe−O26 93.43(3), and O26−C26−O27 125.64(18).

presence of formic acid causes significant structural perturbation to the ($^{iPr}PP^{Me}P$)Fe fragment, including a substantial elongation of the Fe−$P_{central}$ bond and a considerable expansion of the $P_{periphery}$−Fe−$P_{periphery}$ angle (Table 2). These specific structural parameters are, in fact, comparable to those determined for **1**, which, among the iron complexes studied here, possesses the most sterically demanding coordination environment.

Additional mechanistic insights were unveiled when the isolated **5b** (containing a small amount of HCO_2H) was subjected to the decarboxylation study. At room temperature, **5b** (in C_6D_6) slowly decayed to give **3** and CO_2, although the reaction could be greatly accelerated by raising the temperature to 80 °C. Interestingly, **5a** and the free ligand $^{iPr}PP^{Me}P$ did not form under these conditions. Because **5b** and **3** share the same geometry for the H−Fe−CO moiety, isomerization of **5b** to **5a** prior to decarboxylation is not needed. The absence of free ligand suggests that the decomposition described earlier is due to the presence of isomer **5a** or more likely the excess HCO_2H. The predominance of isomer **5b** in the protonation and

https://doi.org/10.1021/acs.inorgchem.2c03803
Inorg. Chem. 2023, 62, 967−978

Table 2. Variation of the Fe−P Bonds and $P_{periphery}$−Fe−$P_{periphery}$ Angle

	Fe−$P_{central}$(Å)	Fe−$P_{periphery}$(Å)	$P_{periphery}$−Fe−$P_{periphery}$(deg)
($^{iPr}PP^{Me}P$)Fe(CO)Cl_2 (**1**)[a]	2.2238(11)	2.2777(10),2.2878(10)	163.36(4)
	2.2253(12)	2.2737(11),2.2894(11)	163.79(4)
($^{iPr}PP^{Me}P$)FeH(CO)Cl (**2a**)	2.1875(10)	2.1956(11),2.2024(10)	152.07(4)
($^{iPr}PP^{Me}P$)FeH(CO)Cl (**2b**)	2.1443(7)	2.2052(8),2.2255(7)	145.73(3)
($^{iPr}PP^{Me}P$)Fe(CO)H_2 (**3**)[a]	2.1392(3)	2.1564(3),2.1619(3)	151.157(14)
	2.1444(3)	2.1566(4),2.1592(3)	154.667(14)
($^{iPr}PP^{Me}P$)FeH(CO)(SCHS) (**4b**)	2.1499(5)	2.2189(3),2.2190(3)	152.700(19)
($^{iPr}PP^{Me}P$)FeH(CO)(OCHO) (**5a**)	2.2238(4)	2.2288(4),2.2296(4)	160.084(17)

[a]Two dependent molecules, hence two sets of data.

Table 3. Dehydrogenation of Formic Acid Catalyzed by Different Iron Complexes[a]

$$HCO_2H \xrightarrow[1,4\text{-dioxane, } 80^\circ C]{0.1\ mol\%[Fe]} H_2 + CO_2$$

entry	[Fe]	TOF_{1h} (conv.)[d,e]	TON_{max}(time, conv.)[e,g]
1	*cis*-($^{iPr}PP^{Me}P$)Fe(CO)H_2 (**3**)	439 (44%)	768 (8 h, 77%)
2[b]	*cis*-($^{iPr}PP^{Me}P$)Fe(CO)H_2 (**3**)	481 (48%)	773 (8 h, 77%)
3[c]	*cis*-($^{iPr}PP^{H}P$)Fe(CO)H_2	473 (47%)	859 (8 h, 86%)
4[b,c]	*cis*-($^{iPr}PP^{H}P$)Fe(CO)H_2	460 (46%)	864 (8 h, 86%)
5	($^{iPr}PP^{Me}P$)FeH(CO)Cl (**2a**)	15 (2%)	15 (1 h, 2%)
6	*trans*-($^{iPr}PP^{Me}P$)Fe(CO)Cl_2 (**1**)	N.R.[f]	N.R.[f]

[a]Standard conditions: HCO_2H (100 μL, 98−100% purity, 2.65 mmol) and an iron catalyst (0.1 mol %) mixed in 1,4-dioxane (0.5 mL). [b]HCO_2H with a purity of 88% was used (100 μL, 2.33 mmol). [c]Reported in ref 4. [d]TOF_{1h} is the calculated turnover frequency after 1 h. [e]Average of two runs. [f]N.R. = no reaction. [g]TON_{max} is the turnover number obtained when the gas production ceased.

isomerization reactions (Scheme 8) highlights the differences between the two PPP systems. The *trans* H−Fe−CO isomer was not detected in the reaction of *cis*-($^{iPr}PP^{H}P$)Fe(CO)H_2 with HCO_2H. The methyl group introduced to the central phosphorus appears to discourage the formate ligand (or its hydrogen-bonding network) from approaching the adjacent coordination site. The **5a**/**5b** ratio of 24:76 shown in Scheme 8 is identical to the ratio for the two dithioformate complexes **4a** and **4b** in equilibrium (Scheme 7), indicating that the protonation reaction was presumably under thermodynamic control.

Catalytic Dehydrogenation of Formic Acid. The steps illustrated in Scheme 8 close a catalytic cycle for the dehydrogenation of formic acid to CO_2. Indeed, dihydride complex **3** was shown to catalyze this reaction at 80−90 °C. The detailed reaction optimization is summarized in the Supporting Information (Table S1). The catalytic reaction can be conducted in 1,4-dioxane, propylene carbonate, 2-propanol, *tert*-butyl alcohol, or *tert*-amyl alcohol with a turnover number (TON) typically measured in the range of 730−865. The studies by Bernskoetter, Hazari, and Schneider focusing on PNP-ligated iron complexes have shown that for the formic acid dehydrogenation reaction Lewis acids such as $LiBF_4$ can enhance the catalytic activity.[2d,20] The two PPP systems presented herein are, however, incompatible with $LiBF_4$; control experiments confirmed that $LiBF_4$ rapidly degraded the iron complexes.

For comparison purposes, we chose reaction conditions (80 °C, in 1,4-dioxane, 0.1 mol % catalyst loading) that were previously optimized for *cis*-($^{iPr}PP^{H}P$)Fe(CO)H_2.[4] As shown in Table 3, dihydride complex **3** catalyzes the dehydrogenation reaction with a turnover frequency (TOF) of 439 h^{-1} measured after 1 h and a maximum TON of 768 achieved in 8 h (entry 1). Using a lower-grade but less-expensive formic acid (88% purity) gives similar TOF_{1h} and TON_{max} (entry 2), implying that the reaction can tolerate a small amount of water. Comparing **3** with *cis*-($^{iPr}PP^{H}P$)Fe(CO)H_2 (entries 1−4) suggests that these two PPP catalytic systems have very similar initial rates of dehydrogenation. The slightly higher TON_{max} values for the $^{iPr}PP^{H}P$ system likely reflect a higher stability of the catalytic species in the acidic medium. The room-temperature reaction of **3** (or *cis*-($^{iPr}PP^{H}P$)Fe(CO)H_2) with a large excess of HCO_2H indicates that the formate complexes are the resting state of the catalyst. Qualitatively, **5b** undergoes room-temperature decarboxylation at a rate slightly slower than for ($^{iPr}PP^{H}P$)FeH(CO)(OCHO),[21] although we suspect that at 80 °C the difference in decarboxylation rates is even smaller. As dihydride complexes, both **3** and *cis*-($^{iPr}PP^{H}P$)Fe(CO)H_2 utilize only one hydride ligand for the protonation step while leaving the other ligand intact. Consistent with this observation, monohydride complex **2a** shows limited catalytic activity (entry 5) whereas dichloride complex **1** does not catalyze the dehydrogenation process at all (entry 6). Overall, **3** and *cis*-($^{iPr}PP^{H}P$)Fe(CO)H_2 represent one of the very few iron-based catalytic systems for the additive-free dehydrogenation of formic acid.[19c,22]

CONCLUSIONS

Through the PPP ligand platform, we have demonstrated the complicated roles that a methyl group can play near the coordination sphere of iron. The net methyl effects on a stoichiometric or catalytic process are reaction-specific. *cis*-($^{iPr}PP^{H}P$)Fe(CO)H_2 catalyzes the conversion of PhCHO to $PhCO_2CH_2Ph$, likely via species degraded from the dihydride complex. The methylated compound, *cis*-($^{iPr}PP^{Me}P$)Fe(CO)H_2 (**3**), is thermally more robust, displaying no catalytic activity for this reaction. Both *cis*-($^{iPr}PP^{H}P$)Fe(CO)H_2 and **3** participate in an insertion reaction with CS_2. The $^{iPr}PP^{H}P$ system is slightly more reactive, which reflects the transition-state instead of the ground-state structure (i.e., ligand

https://doi.org/10.1021/acs.inorgchem.2c03803
Inorg. Chem. 2023, 62, 967−978

reorganization is required). The crystallographic studies suggest that the PPP ligand framework makes adjustments readily to accommodate new ligands with different sizes and *trans* influences. As shown in Table 2, these structural changes can sometimes be fairly substantial, involving Fe−P bond contraction/elongation of as large as 0.13 Å and $P_{periphery}$−Fe−$P_{periphery}$ angle compression/expansion of up to 18.1°. For the dehydrogenation of formic acid, *cis*-($^{iPr}PP^{H}P$)Fe(CO)H_2 and **3** exhibit very similar catalytic activity as far as the initial rates are concerned. However, *cis*-($^{iPr}PP^{H}P$)Fe(CO)H_2 gives a slightly higher TON_{max} value, which we attribute to its higher stability against the acid.

The results obtained from the CS_2 insertion and formic acid dehydrogenation studies would normally be interpreted as proof that the PH hydrogen is chemically innocent or noncooperative.[2] This assertion holds true here; however, the methyl effects are much more complex. In particular, introducing the methyl group to the central phosphorus donor changes the energy landscape of the geometric isomers, resulting in different stereochemistry displayed by the two PPP systems. Two general trends have been noted for the methylated compounds. First, isomers with a *syn* Me−P−Fe−H configuration are not favorable due to the absence of or diminished electrostatic attraction between the methyl group and the hydride. The *anti* configuration, on the other hand, has the advantage of folding the PPP ligand framework so that the hydride is placed in the smaller binding pocket. Second, isomers with *trans*-H−Fe−CO geometry become more favorable when the X-type ligand (Cl, SCHS, OCHO) is sizable enough to experience steric repulsion from the PMe methyl group. Collectively, these factors contribute to the high selectivity observed for the CS_2 insertion reaction with **3**. We believe that the implications of the methyl effects go beyond the PPP ligand system presented here, which will be the subject of our future study.

EXPERIMENTAL SECTION

General Methods. Unless otherwise noted, all organometallic compounds were prepared and handled under an argon atmosphere using standard glovebox and Schlenk techniques. Dry and oxygen-free THF, toluene, and pentane were collected from an Innovative Technology solvent purification system and used throughout the experiments. 2-Propanol, *tert*-butyl alcohol, *tert*-amyl alcohol, propylene carbonate, and 1,4-dioxane were dried over 4 Å molecular sieves and deoxygenated by bubbling argon through them for 1 h prior to use. Formic acid (98−100%) was purchased from Sigma-Aldrich, and a lower-grade formic acid (88%) was purchased from Fisher Scientific; both were deoxygenated via freeze−pump−thaw cycles. Benzene-d_6 (99.5% D) and benzene were dried over sodium benzophenone and distilled under an argon atmosphere. CD_2Cl_2 (99.8% D), toluene-d_8 (99.5% D), and ethanol-d_6 (99% D, anhydrous) were purchased from Cambridge Isotope Laboratories, Inc. Deuterium gas (99.8% D) was purchased from Sigma-Aldrich. These isotopically labeled reagents were used as received without further purification. $^{iPr}PP^{Me}P$[8] and *cis*-($^{iPr}PP^{H}P$)Fe(CO)H_2[4] were prepared as described in the literature. NMR spectra were recorded on a Bruker AV400 or a Bruker NEO400 NMR spectrometer. The chemical shift values for ^{1}H and $^{13}C\{^1H\}$ NMR spectra were referenced internally to the residual solvent resonances. $^{31}P\{^1H\}$ NMR spectra were referenced externally to 85% H_3PO_4 (0 ppm). Infrared spectra were recorded on a PerkinElmer Spectrum Two Fourier transform infrared spectrometer equipped with a Smart Orbit diamond attenuated total reflectance (ATR) accessory.

*Synthesis of trans-($^{iPr}PP^{Me}P$)Fe(CO)Cl_2 (**1**).* In a glovebox, to an oven-dried 100 mL Schlenk flask equipped with a stir bar were added $^{iPr}PP^{Me}P$ (412 mg, 0.95 mmol), $FeCl_2$ (121 mg, 0.95 mmol), and THF (50 mL) with continuous stirring. A dark-maroon precipitate formed immediately. After 1 h, the flask was taken out of the glovebox and connected to a Schlenk line. The argon inside the flask was removed via a freeze−pump−thaw cycle and replaced with CO (1 bar). The precipitate gradually dissolved, forming a light-maroon solution within 15 min. The reaction mixture was stirred for another 15 min, after which the volatiles were removed under vacuum. Washing the residue with pentane (3 × 15 mL) followed by drying under vacuum yielded the desired product as a lilac-colored powder (535 mg, 96% yield). X-ray-quality crystals were grown from THF−pentane at −30 °C. ^{1}H NMR (400 MHz, CD_2Cl_2): δ 8.24 (t, J = 7.0 Hz, Ar*H*, 2H), 7.91−7.80 (m, Ar*H*, 2H), 7.68−7.56 (m, Ar*H*, 4H), 3.47−3.31 (m, C*H*$(CH_3)_2$, 2H), 3.04−2.87 (m, C*H*$(CH_3)_2$, 2H), 1.82 (d, $^2J_{H-P}$ = 10.8 Hz, PCH_3, 3H), 1.73−1.61 (m, CH(CH_3)$_2$, 6H), 1.60−1.50 (m, CH(CH_3)$_2$, 6H), 1.42−1.29 (m, CH(CH_3)$_2$, 6H), 1.17−1.04 (m, CH(CH_3)$_2$, 6H). $^{13}C\{^1H\}$ NMR (101 MHz, CD_2Cl_2): δ 214.8 (q, $^2J_{C-P}$ = 29.3 Hz, CO), 146.3 (dt, J = 48.5 and 16.2 Hz, ArC bonded to P), 143.4 (dt, J = 32.3 and 15.2 Hz, ArC bonded to P), 132.2 (d, J = 15.2 Hz, ArC), 130.8−130.6 (m, ArC), 129.8 (t, J = 5.1 Hz, ArC), 28.5 (t, J = 8.1 Hz, CH(CH$_3$)$_2$), 27.1 (td, J = 9.1 and 2.0 Hz, CH(CH$_3$)$_2$), 20.7 (s, CH(CH_3)$_2$), 19.9 (s, CH(CH_3)$_2$), 19.32 (s, CH(CH_3)$_2$), 19.25 (d, $^1J_{C-P}$ = 27.5 Hz, PCH_3), 19.19 (s, CH(CH_3)$_2$). $^{31}P\{^1H\}$ NMR (162 MHz, CD_2Cl_2): δ 98.1 (t, $^2J_{P-P}$ = 35.6 Hz, PCH_3, 1P), 70.2 (d, $^2J_{P-P}$ = 35.6 Hz, P^{i}Pr$_2$, 2P). Selected ATR-IR data (solid, cm^{-1}): 2959, 2928, 2871, 1962 ($\nu_{C\equiv O}$), 1457, 1429, 1378, 1363. Selected transmission-IR data (CH_2Cl_2, cm^{-1}): 3046, 2965, 2931, 2875, 1946 ($\nu_{C\equiv O}$), 1461, 1429. Anal. Calcd for $C_{26}H_{39}OP_3Cl_2Fe$: C, 53.18; H, 6.69; Cl, 12.07. Found: C, 53.34; H, 6.67; Cl, 11.94.

*Synthesis of ($^{iPr}PP^{Me}P$)FeH(CO)Cl (**2**).* In a glovebox, to an oven-dried 100 mL Schlenk flask equipped with a stir bar were added **1** (100 mg, 0.17 mmol) and $NaBH_4$ (6.5 mg, 0.17 mmol). The flask was taken out of the glovebox, connected to a Schlenk line, and cooled in an ice bath. After 5 min, 15 mL of chilled (0 °C), dry, deoxygenated ethanol was added with continuous stirring. The resulting mixture was slowly warmed to room temperature and stirred overnight. Removal of the volatiles under vacuum gave a brown residue, which was redissolved in 60 mL of toluene and filtered through a pad of Celite. The filtrate was evaporated to dryness under vacuum, giving a mixture of **2a** and **2b** as a brown solid (70 mg, 74% yield). A C_6D_6 solution of this mixture (in a J. Young NMR tube) left standing in a glovebox for 2 months produced single crystals of **2b**.

Pure isomer **2a** was obtained by recrystallization from toluene−pentane at −30 °C, which also produced crystals suitable for X-ray crystallographic study. ^{1}H NMR (400 MHz, CD_2Cl_2): δ 8.34 (t, J = 6.8 Hz, Ar*H*, 2H), 7.77−7.69 (m, Ar*H*, 2H), 7.65−7.58 (m, Ar*H*, 2H), 7.57−7.50 (m, Ar*H*, 2H), 2.91−2.78 (m, C*H*$(CH_3)_2$, 2H), 2.76−2.64 (m, C*H*$(CH_3)_2$, 2H), 1.82 (d, $^2J_{H-P}$ = 9.2 Hz, PCH_3, 3H), 1.41−1.33 (m, CH(CH_3)$_2$, 6H), 1.33−1.25 (m, CH(CH_3)$_2$, 6H), 1.06−0.99 (m, CH(CH_3)$_2$, 6H), 0.93−0.86 (m, CH(CH_3)$_2$, 6H), −26.69 (td, $^2J_{H-P}$ = 56.0 and 47.2 Hz, Fe*H*, 1H). $^{13}C\{^1H\}$ NMR (101 MHz, CD_2Cl_2): δ 225.4−224.7 (m, CO), 147.1 (dt, J = 43.4 and 21.2 Hz, ArC bonded to P), 146.2 (dt, J = 42.4 and 19.2 Hz, ArC bonded to P), 130.6 (d, J = 5.1 Hz, ArC), 130.4−130.3 (m, ArC), 129.9−129.6 (m, ArC), 31.2 (t, J = 6.1 Hz, CH(CH$_3$)$_2$), 29.6 (td, J = 15.2 and 5.1 Hz, CH(CH$_3$)$_2$), 19.8 (s, CH(CH_3)$_2$), 19.04 (t, J = 2.0 Hz, CH(CH_3)$_2$), 18.96 (s, CH(CH_3)$_2$), 18.92 (s, CH(CH_3)$_2$), 16.8 (d, $^1J_{C-P}$ = 24.2 Hz, PCH_3). $^{31}P\{^1H\}$ NMR (162 MHz, CD_2Cl_2): δ 104.1 (AB_2 spin, J_{AB} = 46.4 Hz, P^{i}Pr$_2$, 2P), 100.2 (AB_2 spin, J_{AB} = 46.4 Hz, PCH_3, 1P). Selected ATR-IR data (solid, cm^{-1}): 2866, 1904, 1850, 1458, 1380, 1244, 1113. Anal. Calcd for $C_{26}H_{40}OP_3ClFe$: C, 56.49; H, 7.29; Cl, 6.41. Found: C, 56.34; H, 7.30; Cl, 6.59.

In CD_2Cl_2, **2a** slowly isomerized to **2b**, reaching equilibrium (**2a**/**2b** = 37:63) after it was held at 50 °C for 48 h. During the isomerization process, a third isomer **2c** was also detected, although it represented a very small fraction of the total iron species (<2%). ^{1}H NMR of **2b** (400 MHz, CD_2Cl_2): δ 8.14−8.04 (m, Ar*H*, 2H), 7.93−7.83 (m, Ar*H*, 2H), 7.58−7.48 (m, Ar*H*, 4H), 3.39−3.20 (m, C*H*$(CH_3)_2$, 2H), 2.91−2.75 (m, C*H*$(CH_3)_2$, 2H), 1.56−1.43 (m, CH(CH_3)$_2$ and PCH_3, 15H), 1.16−1.07 (m, CH(CH_3)$_2$, 6H), 0.86−

https://doi.org/10.1021/acs.inorgchem.2c03803
Inorg. Chem. 2023, 62, 967−978

0.77 (m, $CH(CH_3)_2$, 6H), −7.32 (dt, $^2J_{H-P}$ = 59.6 and 54.8 Hz, Fe*H*, 1H). $^{31}P\{^1H\}$ NMR of **2b** (162 MHz, CD_2Cl_2): δ 110.6 (t, J_{P-P} = 31.6 Hz, *P*CH_3, 1P), 101.4 (d, J_{P-P} = 31.6 Hz, *P*^{i}Pr$_2$, 2P). Selected ^1H NMR data of **2c** (400 MHz, CD_2Cl_2): δ −25.61 (dt, $^2J_{H-P}$ = 67.6 and 39.2 Hz, Fe*H*, 1H). $^{31}P\{^1H\}$ NMR of **2c** (162 MHz, CD_2Cl_2): δ 109.0 (d, J_{P-P} = 43.2 Hz, *P*^{i}Pr$_2$, 2P), 100.2 (t, J_{P-P} = 43.2 Hz, *P*CH_3, 1P).

Synthesis of cis-(^{iPr}*PP*^{Me}*P)Fe(CO)H*$_2$ *(**3**).* In a glovebox, to an oven-dried 100 mL Schlenk flask equipped with a stir bar were added **1** (482 mg, 0.82 mmol) and $NaBH_4$ (155 mg, 4.10 mmol). The flask was removed from the glovebox, connected to a Schlenk line, and cooled in an ice bath. After 5 min, 50 mL of chilled (0 °C), dry, deoxygenated ethanol was added with continuous stirring. The resulting mixture was slowly warmed to room temperature and stirred for 24 h. Removal of the volatiles under vacuum gave an orange residue, which was redissolved in 50 mL of toluene and filtered through a pad of Celite. The filtrate was evaporated to dryness under vacuum, affording the desired product as an orange solid (375 mg, 88% yield). X-ray-quality crystals were grown from toluene−pentane or from a saturated pentane solution kept at −30 °C. ^1H NMR (400 MHz, C_6D_6): δ 7.95−7.81 (m, Ar*H*, 2H), 7.36−7.26 (m, Ar*H*, 2H), 7.14−7.02 (m, Ar*H*, 4H), 2.46−2.33 (m, C*H*$(CH_3)_2$, 2H), 2.32−2.20 (m, C*H*$(CH_3)_2$, 2H), 1.82 (d, $^2J_{H-P}$ = 6.4 Hz, PC*H*$_3$, 3H), 1.56−1.42 (m, CH$(CH_3)_2$, 6H), 1.36−1.24 (m, CH$(CH_3)_2$, 6H), 1.01−0.88 (m, CH$(CH_3)_2$, 6H), 0.82−0.65 (m, CH$(CH_3)_2$, 6H), −9.96 (br, Fe*H trans* to CO, 1H), −13.99 (br, Fe*H trans* to the central phosphorus, 1H). Selected ^1H NMR data at −30 °C (400 MHz, toluene-d_8): δ −9.97 (tdd, $^2J_{H-P}$ = 48.3 and 35.8 Hz, $^2J_{H-H}$ = 11.7 Hz, Fe*H trans* to CO, 1H), δ −14.09 (tdd, $^2J_{H-P}$ = 56.6 and 34.6 Hz, $^2J_{H-H}$ = 11.7 Hz, Fe*H trans* to the central phosphorus, 1H). $^{13}C\{^1H\}$ NMR (101 MHz, C_6D_6): δ 221.7 (td, $^2J_{C-P}$ = 12.1 and 9.1 Hz, *C*O), 150.7 (dt, J = 37.4 and 19.2 Hz, Ar*C* bonded to P), 149.5 (ddd, J = 46.3, 17.7, and 16.8 Hz, Ar*C* bonded to P), 129.1−128.5 (m, Ar*C*), 32.6 (t, J = 6.2 Hz, *C*H$(CH_3)_2$), 26.8 (td, J = 16.4 and 7.0 Hz, *C*H$(CH_3)_2$), 21.6 (d, $^1J_{C-P}$ = 20.6 Hz, PCH_3), 19.9 (t, J = 3.0 Hz, CH$(CH_3)_2$), 19.8 (t, J = 3.3 Hz, CH$(CH_3)_2$), 19.6 (s, CH$(CH_3)_2$), 18.7 (s, CH$(CH_3)_2$). $^{31}P\{^1H\}$ NMR (162 MHz, C_6D_6): δ 127.1 (d, $^2J_{P-P}$ = 21.4 Hz, *P*^{i}Pr$_2$, 2P), 100.8 (t, $^2J_{P-P}$ = 21.4 Hz, *P*CH_3, 1P). Selected ATR-IR data (solid, cm^{-1}): 2949, 2919, 2864, 1899, 1858, 1824, 1461, 1440, 1425, 1376, 1358, 1261, 1237, 1104. Anal. Calcd for $C_{26}H_{41}OP_3Fe$: C, 60.24; H, 7.97. Found: C, 60.43; H, 8.07.

Synthesis of (^{iPr}*PP*^{Me}*P)FeH(CO)(SCHS) (**4b**).* In a glovebox, to a screw-cap NMR tube were added **3** (25 mg, 48 μmol), carbon disulfide (5.8 μL, 96 μmol), and 1 mL of C_6D_6. The tube was sealed with a PTFE/silicone septum, taken out of the glovebox, and inserted into an NMR heating block with the temperature set to 80 °C. The progress of the reaction was monitored by NMR spectroscopy. When the reaction was complete (∼18 h), the volatiles were removed by purging the solution with argon. The resulting solid was subject to recrystallization in toluene−THF at −30 °C, giving pure **4b** in the form of bright-orange crystals (15 mg, 45% yield). The synthesis was also repeated using benzene as the solvent with 1 drop of C_6D_6 being added to lock the NMR signal. ^1H NMR (400 MHz, CD_2Cl_2): δ 11.81 (s, SC*H*S, 1H), 8.22 (t, J = 7.0 Hz, Ar*H*, 2H), 7.89−7.77 (m, Ar*H*, 2H), 7.67−7.50 (m, Ar*H*, 4H), 3.10−2.92 (m, C*H*$(CH_3)_2$, 2H), 2.83−2.66 (m, C*H*$(CH_3)_2$, 2H), 1.72 (d, $^2J_{H-P}$ = 8.3 Hz, PC*H*$_3$, 3H), 1.52−1.39 (m, CH$(CH_3)_2$, 6H), 1.38−1.24 (m, CH$(CH_3)_2$, 6H), 1.16−1.03 (m, CH$(CH_3)_2$, 6H), 0.94−0.78 (m, CH$(CH_3)_2$, 6H), −9.03 (q, $^2J_{H-P}$ = 52.8 Hz, Fe*H*, 1H). ^1H NMR (400 MHz, C_6D_6): δ 12.58 (s, SC*H*S, 1H), 7.61 (t, J = 6.8 Hz, Ar*H*, 2H), 7.34−7.28 (m, Ar*H*, 2H), 7.03−6.95 (m, Ar*H*, 4H), 3.16−2.98 (m, C*H*$(CH_3)_2$, 2H), 2.50−2.32 (m, C*H*$(CH_3)_2$, 2H), 1.44 (d, $^2J_{H-P}$ = 8.0 Hz, PC*H*$_3$, 3H), 1.40−1.32 (m, CH$(CH_3)_2$, 6H), 1.17−1.05 (m, CH$(CH_3)_2$, 12H), 0.79−0.68 (m, CH$(CH_3)_2$, 6H), −9.17 (q, $^2J_{H-P}$ = 52.8 Hz, Fe*H*, 1H). $^{13}C\{^1H\}$ NMR (101 MHz, CD_2Cl_2): δ 243.1−242.7 (m, SCHS), 219.1−218.6 (m, *C*O), 147.3 (dt, J = 46.7 and 17.0 Hz, Ar*C* bonded to P), 145.5 (ddd, J = 37.4, 19.3, and 18.7 Hz, Ar*C* bonded to P), 131.0−130.7 (m, Ar*C*), 130.6 (d, J = 5.4 Hz, Ar*C*), 130.3 (d, J = 16.2 Hz, Ar*C*), 129.2 (t, J = 6.2 Hz, Ar*C*), 29.7 (t, J = 7.8 Hz, *C*H$(CH_3)_2$), 25.5 (td, J = 13.9 and 2.6 Hz, *C*H$(CH_3)_2$), 22.9 (d, $^1J_{C-P}$ = 28.6 Hz, PCH_3), 18.9 (s, CH$(CH_3)_2$), 18.74 (t, J = 2.2 Hz, CH$(CH_3)_2$), 18.66 (t, J = 2.9 Hz, CH$(CH_3)_2$), 18.5 (s, CH$(CH_3)_2$). $^{31}P\{^1H\}$ NMR (162 MHz, CD_2Cl_2): δ 106.2 (t, $^2J_{P-P}$ = 29.2 Hz, *P*CH_3, 1P), 99.1 (d, $^2J_{P-P}$ = 29.2 Hz, *P*^{i}Pr$_2$, 2P). $^{31}P\{^1H\}$ NMR (162 MHz, C_6D_6): δ 106.4 (t, $^2J_{P-P}$ = 28.4 Hz, *P*CH_3, 1P), 99.8 (d, $^2J_{P-P}$ = 28.4 Hz, *P*^{i}Pr$_2$, 2P). Selected ATR-IR data (solid, cm^{-1}): 2961, 2929, 2870, 1919, 1874, 1460, 1428, 1382, 1363, 1282, 1237 (ν_{HCS}), 1113, 986 (ν_{CS_2}). Anal. Calcd for $C_{27}H_{41}OS_2P_3Fe{\cdot}C_7H_8$: C, 59.47; H, 7.19. Found: C, 59.57; H, 7.25.

In C_6D_6, **4b** slowly isomerized to **4a**, reaching equilibrium (**4a**/**4b** = 25:75) after it was held at 80 °C for 24 h. ^1H NMR of **4a** (400 MHz, C_6D_6): δ 12.55 (s, SC*H*S, 1H), 7.78 (t, J = 6.8 Hz, Ar*H*, 2H), 7.08−6.94 (m, Ar*H*, 6H), 2.75−2.58 (m, C*H*$(CH_3)_2$, 4H), 1.74 (d, $^2J_{H-P}$ = 8.0 Hz, PC*H*$_3$, 3H), 1.49−1.40 (m, CH$(CH_3)_2$, 6H), 1.08−1.02 (m, CH$(CH_3)_2$, 6H), 0.95−0.81 (m, CH$(CH_3)_2$, 12H), −19.22 (td, $^2J_{H-P}$ = 53.6 and 46.0 Hz, Fe*H*, 1H). $^{31}P\{^1H\}$ NMR of **4a** (162 MHz, C_6D_6, δ): 104.7 (d, $^2J_{P-P}$ = 41.6 Hz, *P*^{i}Pr$_2$, 2P), 95.6 (t, $^2J_{P-P}$ = 41.6 Hz, *P*CH_3, 1P).

Synthesis of (^{iPr}*PP*^{Me}*P)FeH(CO)(OCHO)·(HCO*$_2$*H)*$_x$ *(**5**·(HCO*$_2$*H)*$_x$*).* In a glovebox, to an oven-dried 10 mL Schlenk tube equipped with a stir bar were added **3** (25 mg, 48 μmol) and 0.5 mL of 1,4-dioxane. The tube was sealed with a rubber septum, removed from the glovebox, and connected to a Schlenk line under argon. Formic acid (22 μL, 98−100% purity, 0.58 mmol) was added via a microliter syringe, and the reaction mixture was left stirring for 5 min, after which the volatiles were removed under vacuum. The resulting orange solid was subject to recrystallization in toluene−THF at −30 °C. The first crop of precipitate formed in a week, which was separated by decanting off the mother liquor and identified as **5b**·$(HCO_2H)_x$ (16 mg, ∼55% yield. The solid sample was amorphous, characterized by NMR and IR spectroscopy as well as elemental analysis. The mother liquor was kept at −30 °C, producing single crystals in weeks. They were identified as **5a**·$(HCO_2H)_2$ by X-ray crystallography. ^1H NMR of **5b**·$(HCO_2H)_x$ (400 MHz, C_6D_6): δ 8.85 (s, OC*H*O, 1H), 7.58−7.46 (m, Ar*H*, 2H), 7.39−7.27 (m, Ar*H*, 2H), 7.05−6.94 (m, Ar*H*, 4H), 2.79−2.59 (m, C*H*$(CH_3)_2$, 2H), 2.48−2.31 (m, C*H*$(CH_3)_2$, 2H), 1.43−1.31 (m, CH$(CH_3)_2$, 6H), 1.30−1.10 (m, CH$(CH_3)_2$ and PCH_3, 15H), 0.84−0.69 (m, CH$(CH_3)_2$, 6H), −5.86 (dt, $^2J_{H-P}$ = 62.4 and 52.8 Hz, Fe*H*, 1H); the hydrogen-bonded HCO_2H (14.23 and 8.43 ppm) was also present in a freshly prepared sample. Acquisition of the $^{13}C\{^1H\}$ NMR spectrum was complicated by the decarboxylation of **5b**·$(HCO_2H)_x$ to yield **3** and CO_2 (124.8 ppm). $^{31}P\{^1H\}$ NMR of **5b**·$(HCO_2H)_x$ (162 MHz, C_6D_6): δ 105.2 (t, $^2J_{P-P}$ = 25.6 Hz, *P*CH_3, 1P), 101.3 (d, $^2J_{P-P}$ = 27.0 Hz, *P*^{i}Pr$_2$, 2P); **3** was also present during NMR acquisition. Selected ATR-IR data of **5b**·$(HCO_2H)_x$ (solid, cm^{-1}): 2960, 2929, 2870, 1909, 1717 (ν_{OCO}), 1534, 1494, 1457, 1381, 1343, 1292, 1242, 1203, 1117. Anal. Calcd for $C_{27}H_{41}O_3P_3Fe$ (**5b**): C, 57.66; H, 7.35. Anal. Calcd for $C_{28}H_{43}O_5P_3Fe$ (**5b**·HCO_2H): C, 55.28; H, 7.12. Found: C, 56.67; H, 7.46. The carbon content is in between the predicted values for **5** and **5b**·HCO_2H, consistent with the presence of HCO_2H at the time of analysis.

The protonation of **3** (in C_6D_6) with 5.5 equiv of HCO_2H generated **5a**·$(HCO_2H)_x$ as a transient species. Selected ^1H NMR data of **5a**·$(HCO_2H)_x$ (400 MHz, C_6D_6): δ −28.24 shifted to δ −27.85 (q, $^2J_{H-P}$ = 51.6 Hz, Fe*H*, 1H). $^{31}P\{^1H\}$ NMR of **5a**·$(HCO_2H)_x$ (162 MHz, C_6D_6): δ 101.6 shifted to 102.5 (d, $^2J_{P-P}$ = 46.2 Hz, *P*^{i}Pr$_2$, 2P), 97.7 shifted to 98.0 (t, $^2J_{P-P}$ = 46.2 Hz, *P*CH_3, 1P).

Catalytic Dehydrogenation of Formic Acid. In a glovebox, an oven-dried 10 mL Schlenk tube equipped with a stir bar was loaded with an iron catalyst and an appropriate solvent and then sealed with a rubber septum. The tube was taken out of the glovebox and attached to a Chemglass gas evolution measurement apparatus (catalog CG-1818) filled with mineral oil. Formic acid was added via a microliter syringe, and the tube was quickly immersed in a preheated oil bath. The volume of the produced gas was first measured from a change in oil level and then corrected by subtracting out the volume obtained from a blank reaction (without a catalyst). TOF and TON were

https://doi.org/10.1021/acs.inorgchem.2c03803
Inorg. Chem. 2023, 62, 967−978

calculated based on a method that was previously described in the literature.[20,23]

X-ray Structure Determinations. Crystal data collection and refinement parameters are provided in the Supporting Information. The intensity data were collected at 150 K on a Bruker D8 Venture Photon-II diffractometer using Mo Kα radiation, λ = 0.71073 Å. The data frames were processed using the program *SAINT*. The data were corrected for decay, Lorentz, and polarization effects as well as absorption and beam corrections. The structures were solved by a combination of direct methods and the difference Fourier technique as implemented in the *SHELX* suite of programs and refined by full-matrix least squares on F^2 for reflections out to 0.80 Å (for **1**, **2a**, and **2b**) or 0.75 Å (for **3**, **4b**, and **5a**). Non-hydrogen atoms were refined with anisotropic displacement parameters. Hydrogen atoms bound to iron and oxygen were located directly from the difference map, and their coordinates and isotropic displacement parameters were refined. All remaining hydrogen atoms were calculated and treated with a riding model. The isotropic displacement parameters were defined as a^*U_{eq} (a = 1.5 for methyl and hydroxyl, 1.2 for all others) for the adjacent atom. Compounds **1** and **3** crystallize as two independent molecules in the lattice. The former exists as a pseudomeroheral twin (twin law applied: 1 0 0 0 -1 0 0 0 -1, 35.2%). Compound **4b** crystallizes as a toluene solvate. Compound **5a** cocrystallizes with two molecules of formic acid (hydrogen bonded) in the lattice. Crystal structures of **1**, **2a**, **2b**, **3**, **4b**, and **5a** were deposited at the Cambridge Crystallographic Data Centre (CCDC) and assigned the deposition numbers CCDC 2215937−2215942.

■ ASSOCIATED CONTENT

Supporting Information

The Supporting Information is available free of charge at https://pubs.acs.org/doi/10.1021/acs.inorgchem.2c03803.

NMR and IR spectra of the iron complexes, additional experimental details, and more detailed X-ray crystallographic information (PDF)

Accession Codes

CCDC 2215937−2215942 contain the supplementary crystallographic data for this paper. These data can be obtained free of charge via www.ccdc.cam.ac.uk/data_request/cif, or by emailing data_request@ccdc.cam.ac.uk, or by contacting The Cambridge Crystallographic Data Centre, 12 Union Road, Cambridge CB2 1EZ, UK; fax: +44 1223 336033.

■ AUTHOR INFORMATION

Corresponding Author

Hairong Guan − *Department of Chemistry, University of Cincinnati, Cincinnati, Ohio 45221-0172, United States;* orcid.org/0000-0002-4858-3159; Email: hairong.guan@uc.edu

Authors

Bedraj Pandey − *Department of Chemistry, University of Cincinnati, Cincinnati, Ohio 45221-0172, United States*

Jeanette A. Krause − *Department of Chemistry, University of Cincinnati, Cincinnati, Ohio 45221-0172, United States*

Complete contact information is available at: https://pubs.acs.org/10.1021/acs.inorgchem.2c03803

Notes

The authors declare no competing financial interest.

■ ACKNOWLEDGMENTS

We thank the NSF Chemical Catalysis Program for supporting this research project (grant CHE-2102192) and the NSF MRI Program for supporting the instrumentation used in this study, which includes a Bruker D8 Venture diffractometer (grant CHE-1625737) and a Bruker NEO400 MHz NMR spectrometer (grant CHE-1726092). B.P. thanks the University of Cincinnati for a doctoral enhancement research fellowship.

■ REFERENCES

(1) (a) Barreiro, E. J.; Kümmerle, A. E.; Fraga, C. A. M. The Methylation Effect in Medicinal Chemistry. *Chem. Rev.* **2011**, *111*, 5215−5246. (b) Schönherr, H.; Cernak, T. Profound Methyl Effects in Drug Discovery and a Call for New C−H Methylation Reactions. *Angew. Chem., Int. Ed.* **2013**, *52*, 12256−12267.

(2) (a) Zhang, G.; Vasudevan, K. V.; Scott, B. L.; Hanson, S. K. Understanding the Mechanisms of Cobalt-Catalyzed Hydrogenation and Dehydrogenation Reactions. *J. Am. Chem. Soc.* **2013**, *135*, 8668−8681. (b) Werkmeister, S.; Junge, K.; Wendt, B.; Alberico, E.; Jiao, H.; Baumann, W.; Jung, H.; Gallou, F.; Beller, M. Hydrogenation of Esters to Alcohols with a Well-Defined Iron Complex. *Angew. Chem., Int. Ed.* **2014**, *53*, 8722−8726. (c) Bornschein, C.; Werkmeister, S.; Wendt, B.; Jiao, H.; Alberico, E.; Baumann, W.; Junge, H.; Junge, K.; Beller, M. Mild and Selective Hydrogenation of Aromatic and Aliphatic (Di)nitriles with a Well-Defined Iron Pincer Complex. *Nat. Commun.* **2014**, *5*, 4111. (d) Zhang, Y.; MacIntosh, A. D.; Wong, J. L.; Bielinski, E. A.; Williard, P. G.; Mercado, B. Q.; Hazari, N.; Bernskoetter, W. H. Iron Catalyzed CO_2 Hydrogenation to Formate Enhanced by Lewis Acid Co-Catalysts. *Chem. Sci.* **2015**, *6*, 4291−4299. (e) Yuwen, J.; Chakraborty, S.; Brennessel, W. W.; Jones, W. D. Additive-Free Cobalt-Catalyzed Hydrogenation of Esters to Alcohols. *ACS Catal.* **2017**, *7*, 3735−3740. (f) Curley, J. B.; Smith, N. E.; Bernskoetter, W. H.; Hazari, N.; Mercado, B. Q. Catalytic Formic Acid Dehydrogenation and CO_2 Hydrogenation Using Iron PN^RP Pincer Complexes with Isonitrile Ligands. *Organometallics* **2018**, *37*, 3846−3853. (g) Jayarathne, U.; Hazari, N.; Bernskoetter, W. H. Selective Iron-Catalyzed *N*-Formylation of Amines Using Dihydrogen and Carbon Dioxide. *ACS Catal.* **2018**, *8*, 1338−1345. (h) Yang, W.; Chernyshov, I. Yu; Weber, M.; Pidko, E. A.; Filonenko, G. A. Switching between Hydrogenation and Olefin Transposition Catalysis via Silencing NH Cooperativity in Mn(I) Pincer Complexes. *ACS Catal.* **2022**, *12*, 10818−10825.

(3) Dub, P. A.; Scott, B. L.; Gordon, J. C. Why Does Alkylation of the N−H Functionality within M/NH Bifunctional Noyori-Type Catalysts Lead to Turnover? *J. Am. Chem. Soc.* **2017**, *139*, 1245−1260.

(4) Pandey, B.; Krause, J. A.; Guan, H. Iron Dihydride Complex Stabilized by an All-Phosphorus-Based Pincer Ligand and Carbon Monoxide. *Inorg. Chem.* **2022**, *61*, 11143−11155.

(5) On the basis of the electronegativity values (χ_P = 2.19, χ_H = 2.20, χ_C = 2.55, and χ_{CH_3} = 2.27, Pauling scale), we predict that the methyl group carries less positive charge than the PH hydrogen. For the electronegativity of the methyl group, see Huheey, J. E. The Electronegativity of Groups. *J. Phys. Chem.* **1965**, *69*, 3284−3291.

(6) In a simplified model system, Ph_2PMe proves to be more electron-rich than Ph_2PH, as judged by the electronic parameters or the A_1 carbonyl bands of $Ni(CO)_3L$. For reference, see Tolman, C. A. Steric Effects of Phosphorus Ligands in Organometallic Chemistry and Homogeneous Catalysis. *Chem. Rev.* **1977**, *77*, 313−348.

(7) Dai, H.; Guan, H. Iron Dihydride Complexes: Synthesis, Reactivity, and Catalytic Applications. *Isr. J. Chem.* **2017**, *57*, 1170−1203.

(8) Kim, Y.-E.; Kim, J.; Lee, Y. Formation of a Nickel Carbon Dioxide Adduct and Its Transformation Mediated by a Lewis Acid. *Chem. Commun.* **2014**, *50*, 11458−11461.

(9) Hunter, A. D.; Williams, T. R.; Zarzyczny, B. M.; Bottesch, H. W., II; Dolan, S. A.; McDowell, K. A.; Thomas, D. N.; Mahler, C. H. Correlations among ^{31}P NMR Coordination Chemical Shifts, Ru−P Bond Distances, and Enthalpies of Reaction in $Cp'Ru(PR_3)_2Cl$ Complexes (Cp' = η^5-C_5H_5, η^5-C_5Me_5; PR_3 = PMe_3, $PPhMe_2$, PPh_2Me, PPh_3, PEt_3, P^nBu_3). *Organometallics* **2016**, *35*, 2701−2706.

(10) The tetrahedral geometry about the central phosphorus causes the ligand framework to fold while creating a smaller binding pocket *anti* to the PMe methyl group or PH hydrogen.
(11) Pelczar, E. M.; Emge, T. J.; Krogh-Jespersen, K.; Goldman, A. S. Unusual Structural and Spectroscopic Features of Some PNP-Pincer Complexes of Iron. *Organometallics* **2008**, *27*, 5759−5767.
(12) (a) Lian, T.; Locke, B.; Kitagawa, T.; Nagai, M.; Hochstrasser, R. M. Determination of Fe−CO Geometry in the Subunits of Carbonmonoxy Hemoglobin M Boston Using Femtosecond Infrared Spectroscopy. *Biochemistry* **1993**, *32*, 5809−5814. (b) Spiro, T. G.; Kozlowski, P. M. Is the CO Adduct of Myoglobin Bent, and Does It Matter? *Acc. Chem. Res.* **2001**, *34*, 137−144.
(13) For iron hydride complexes supported by a pincer-type ligand, the chemical shift value for the hydride is typically associated with its *trans* ligand (CO: δ −6 to −10; phosphines: δ −12 to −16; and chloride: δ −19 to −28). For examples, see (a) Langer, R.; Diskin-Posner, Y.; Leitus, G.; Shimon, L. J. W.; Ben-David, Y.; Milstein, D. Low-Pressure Hydrogenation of Carbon Dioxide Catalyzed by an Iron Pincer Complex Exhibiting Noble Metal Activity. *Angew. Chem., Int. Ed.* **2011**, *50*, 9948−9952. (b) Sonnenberg, J. F.; Wan, K. Y.; Sues, P. E.; Morris, R. H. Ketone Asymmetric Hydrogenation Catalyzed by P-NH-P′ Pincer Iron Catalysts: An Experimental and Computational Study. *ACS Catal.* **2017**, *7*, 316−326. (c) Collett, J. D.; Ransohoff, R. W.; Krause, J. A.; Guan, H. An Iron-Hydrogen Bond Resistant to Protonation and Oxidation. *Z. Anorg. Allg. Chem.* **2021**, *647*, 1449−1454. (d) Bhattacharya, P.; Krause, J. A.; Guan, H. Iron Hydride Complexes Bearing Phosphinite-Based Pincer Ligands: Synthesis, Reactivity, and Catalytic Application in Hydrosilylation Reactions. *Organometallics* **2011**, *30*, 4720−4729. (e) Bhattacharya, P.; Krause, J. A.; Guan, H. Mechanistic Studies of Ammonia Borane Dehydrogenation Catalyzed by Iron Pincer Complexes. *J. Am. Chem. Soc.* **2014**, *136*, 11153−11161. (f) Curley, J. B.; Smith, N. E.; Bernskoetter, W. H.; Ertem, M. Z.; Hazari, N.; Mercado, B. Q.; Townsend, T. M.; Wang, X. Understanding the Reactivity and Decomposition of a Highly Active Iron Pincer Catalyst for Hydrogenation and Dehydrogenation Reactions. *ACS Catal.* **2021**, *11*, 10631−10646. (g) Koehne, I.; Schmeier, T. J.; Bielinski, E. A.; Pan, C. J.; Lagaditis, P. O.; Bernskoetter, W. H.; Takase, M. K.; Würtele, C.; Hazari, N.; Schneider, S. Synthesis and Structure of Six-Coordinate Iron Borohydride Complexes Supported by PNP Ligands. *Inorg. Chem.* **2014**, *53*, 2133−2143. (h) Rivada-Wheelaghan, O.; Dauth, A.; Leitus, G.; Diskin-Posner, Y.; Milstein, D. Synthesis and Reactivity of Iron Complexes with a New Pyrazine-Based Pincer Ligand, and Application in Catalytic Low-Pressure Hydrogenation of Carbon Dioxide. *Inorg. Chem.* **2015**, *54*, 4526−4538. (i) Smith, N. E.; Bernskoetter, W. H.; Hazari, N.; Mercado, B. Q. Synthesis and Catalytic Activity of PNP-Supported Iron Complexes with Ancillary Isonitrile Ligands. *Organometallics* **2017**, *36*, 3995−4004.
(14) Because the $\nu_{C\equiv O}$ and ν_{Fe-H} bands are coupled for the iron hydride complexes, the exact CO stretching frequencies are unknown. For this reason, no attempt was made to compare the $\nu_{C\equiv O}$ bands for different hydride species described in this article.
(15) Dai, H.; Li, W.; Krause, J. A.; Guan, H. Experimental Evidence of *syn* H−N−Fe−H Configurational Requirement for Iron-Based Bifunctional Hydrogenation Catalysts. *Inorg. Chem.* **2021**, *60*, 6521−6535.
(16) Gorgas, N.; Stöger, B.; Veiros, L. F.; Pittenauer, E.; Allmaier, G.; Kirchner, K. Efficient Hydrogenation of Ketones and Aldehydes Catalyzed by Well-Defined Iron(II) PNP Pincer Complexes: Evidence for an Insertion Mechanism. *Organometallics* **2014**, *33*, 6905−6914.
(17) (a) Heinekey, D. M.; Millar, J. M.; Koetzle, T. F.; Payne, N. G.; Zilm, K. W. Structural and Spectroscopic Characterization of Iridium Trihydride Complexes: Evidence for Proton-Proton Exchange Coupling. *J. Am. Chem. Soc.* **1990**, *112*, 909−919. (b) Gusev, D. G.; Kuhlman, R.; Sini, G.; Eisenstein, O.; Caulton, K. G. Distinct Structures for Ruthenium and Osmium Hydrido Halides: $Os(H)_3X(P^iPr_3)_2$ (X = Cl, Br, I) Are Nonoctahedral Classical Trihydrides with Exchange Coupling. *J. Am. Chem. Soc.* **1994**, *116*, 2685−2686. (c) Demachy, I.; Esteruelas, M. A.; Jean, Y.; Lledós, A.; Maseras, F.; Oro, L. A.; Valero, C.; Volatron, F. Hydride Exchange Processes in the Coordination Sphere of Transition Metal Complexes: The $OsH_3(BH_4)(PR_3)_2$ System. *J. Am. Chem. Soc.* **1996**, *118*, 8388−8394.
(18) (a) Pandey, K. K. Reactivities of Carbon Sulfide (COS), Carbon Disulfide (CS_2) and Carbon Dioxide (CO_2) with Transition Metal Complexes. *Coord. Chem. Rev.* **1995**, *140*, 37−114. (b) Field, L. D.; Lawrenz, E. T.; Shaw, W. J.; Turner, P. Insertion of CO_2, CS_2, and COS into Iron(II)−Hydride Bonds. *Inorg. Chem.* **2000**, *39*, 5632−5638. (c) Ma, Q.-Q.; Liu, T.; Adhikary, A.; Zhang, J.; Krause, J. A.; Guan, H. Using CS_2 to Probe the Mechanistic Details of Decarboxylation of Bis(phosphinite)-Ligated Nickel Pincer Formate Complexes. *Organometallics* **2016**, *35*, 4077−4082. (d) Wang, L.; Sun, H.; Zuo, Z.; Li, X.; Xu, W.; Langer, R.; Fuhr, O.; Fenske, D. Activation of CO_2, CS_2 and Dehydrogenation of Formic Acid Catalyzed by Iron(II) Hydride Complexes. *Eur. J. Inorg. Chem.* **2016**, *2016*, 5205−5214.
(19) (a) Zell, T.; Butschke, B.; Ben-David, Y.; Milstein, D. Efficient Hydrogen Liberation from Formic Acid Catalyzed by a Well-Defined Iron Pincer Complex under Mild Conditions. *Chem.—Eur. J.* **2013**, *19*, 8068−8072. (b) Mellone, I.; Gorgas, N.; Bertini, F.; Peruzzini, M.; Kirchner, K.; Gonsalvi, L. Selective Formic Acid Dehydrogenation Catalyzed by Fe-PNP Pincer Complexes Based on the 2,6-Diaminopyridine Scaffold. *Organometallics* **2016**, *35*, 3344−3349. (c) Curley, J. B.; Bernskoetter, W. H.; Hazari, N. Additive-Free Formic Acid Dehydrogenation Using a Pincer-Supported Iron Catalyst. *ChemCatChem.* **2020**, *12*, 1934−1938.
(20) Bielinski, E. A.; Lagaditis, P. O.; Zhang, Y.; Mercado, B. Q.; Würtele, C.; Bernskoetter, W. H.; Hazari, N.; Schneider, S. Lewis Acid-Assisted Formic Acid Dehydrogenation Using a Pincer-Supported Iron Catalyst. *J. Am. Chem. Soc.* **2014**, *136*, 10234−10237.
(21) A quantitative comparison of the two PPP systems is challenging because **5b** and ($^{iPr}PP^HP$)FeH(CO)(OCHO) have variable amounts of HCO_2H hydrogen bonded to the complexes and the $^{iPr}PP^{Me}P$ systems involves two different geometric isomers (**5a** and **5b**).
(22) (a) Bertini, F.; Mellone, I.; Ienco, A.; Peruzzini, M.; Gonsalvi, L. Iron(II) Complexes of the Linear *rac*-Tetraphos-1 Ligand as Efficient Homogeneous Catalysts for Sodium Bicarbonate Hydrogenation and Formic Acid Dehydrogenation. *ACS Catal.* **2015**, *5*, 1254−1265. (b) Montandon-Clerc, M.; Dalebrook, A. F.; Laurenczy, G. Quantitative Aqueous Phase Formic Acid Dehydrogenation Using Iron(II) Based Catalysts. *J. Catal.* **2016**, *343*, 62−67.
(23) (a) Boddien, A.; Mellmann, D.; Gärtner, F.; Jackstell, R.; Junge, H.; Dyson, P. J.; Laurenczy, G.; Ludwig, R.; Beller, M. Efficient Dehydrogenation of Formic Acid Using an Iron Catalyst. *Science* **2011**, *333*, 1733−1736. (b) Lentz, N.; Aloisi, A.; Thuéry, P.; Nicolas, E.; Cantat, T. Additive-Free Formic Acid Dehydrogenation Catalyzed by a Cobalt Complex. *Organometallics* **2021**, *40*, 565−569.

https://doi.org/10.1021/acs.inorgchem.2c03803
Inorg. Chem. 2023, 62, 967−978